Simulation and Characterization of a CMOS Z-axis Microactuator with Electrostatic Comb Drives

Huikai Xie*, Lars Erdmann*, Qi Jing* and Gary K. Fedder*†
*Department of Electrical and Computer Engineering and †The Robotics Institute
Carnegie Mellon University, Pittsburgh, PA 15213, USA
Email: xie@ece.cmu.edu Tel: (412) 268-6607 Fax: (412) 268-4595

ABSTRACT

This paper reports the first design and its simulation and experimental results of a CMOS z-axis microactuator that utilizes the vertical electrostatic forces existing between multi-conductor comb fingers. The measured maximum displacement of the z-axis microactuator is 3.5 μm, and resonant frequency 6.17 kHz, which are in good agreement with the field simulation and the behavioral simulation results using the NODAS library [1]. The advantages of the z-axis actuator include compatibility with standard CMOS processes and easy implementation of 3-axis microstages, integrated position sensing components and motion control circuits.

Keywords: vertical actuation, NODAS library, behavioral simulation, comb drive, CMOS micromachining process

INTRODUCTION

Interdigitated comb drives have been widely used for electrostatic actuation [2], capacitive acceleration or position sensing [3] and frequency tuning [4]. They have become an integral part of many MEMS devices such as accelerometers [3], gyroscopes [5], and microscanners [6]. Most of these devices utilize the lateral capacitance change between comb fingers. Z-axis accelerometer servo-mechanisms and x-y axis vibratory gyroscopes require z-axis (out-of-plane) sensing. Parallel-plate capacitors are commonly used in polysilicon MEMS for this purpose. However, in CMOS MEMS where no underlying electrode is available, an alternate means of sensing out-of-plane motion is needed. Furthermore, 3-axis microstages, and reference mirrors of interferometers must have z-axis actuation. It was found that vertical levitation exists in laterally driven comb-drive actuators [2]. This levitation effect can be used to make vertical comb-drive actuators [7].

In this paper, we describe a new method to realize z-axis comb-drive actuation in a maskless post-CMOS micromachining process [8] which utilizes metal layers from the initial standard CMOS processing as etching masks. The cross-sectional view of the final step of the process-flow is illustrated in Figure 1. There are three important features: (1) compatibility with conventional CMOS processes, (2) small parasitic capacitance to the substrate and elimination of vertical levitation because of the large gap between microstructures and the substrate, and (3) multi-conductor structures with up to three isolated metal layers make it possible to construct more than 20 different capacitor configurations across a single comb finger air gap. One of the configurations for vertical actuation will be discussed in the next section. A CMOS z-axis accelerometer has been previously made by using similar capacitor configurations [9]. In Figure 1, beam-2 is thinner than beam-1, which is realized by choosing metal1 and metal3 as the etching masks, respectively. Therefore, suspensions can be designed more flexible either along a lateral axis or along the vertical axis.

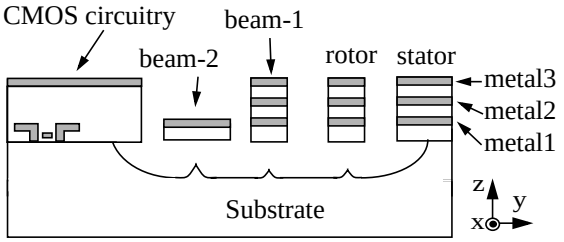

Figure 1: Schematic cross-section of the last step of the post-CMOS micromachining process.

A 3-axis microstage is designed and fabricated in the Hewlett-Packard 3-metal 0.5 μm CMOS process followed by post-CMOS micromachining. The lateral-axis actuators behave the same way as a polysilicon comb drive [3], and this paper will focus on the z-axis actuation. The operational principle of the z-axis comb-finger actuation is briefly introduced first, followed by electrostatic field analysis using the Maxwell 2D simulator [11]. Then the dynamic response is simulated using the NODAS library [1]. Finally, the simulation results are compared with the experimental results. The static and dynamic behaviors of the z-motion are characterized using an interferometeric technique.

Z-AXIS COMB-FINGER ACTUATION

The top view of the fabricated 3-axis microstage is shown in Figure 2. The central proof mass can be driven in all three directions. There is one separate set of comb fingers for each direction. The y- and z-axis comb drives are suspended by a set of springs that are flexible in both y and

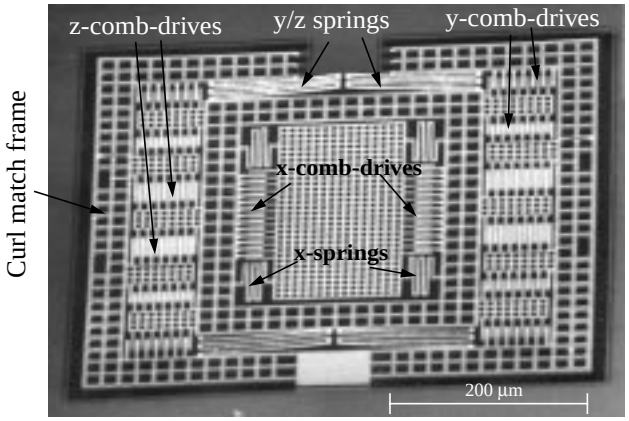

Figure 2: SEM photo of the z-axis actuator (also showing the x- and y- axis actuators).

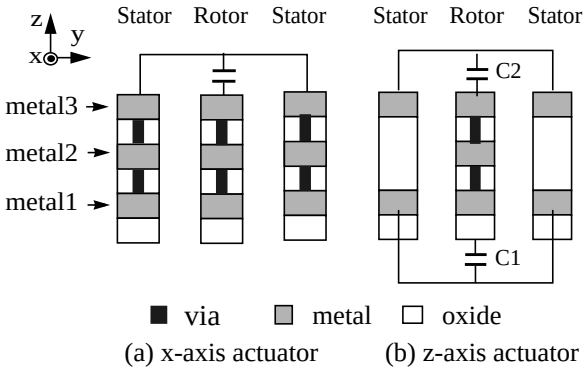

Figure 3: Cross-sections and wiring configurations of CMOS lateral and vertical comb-drives.

z directions. The device curls out of plane about 8 µm at the edges due to residual stress and thermal coefficient mismatch in the multi-layer structures. However, the stationary fingers (stators) and movable fingers (rotors) align very well locally through use of a curl match frame [3].

The cross-sections of the comb fingers are shown in Figure 3. The comb fingers consist of three metal layers and are suspended about 25 µm above the substrate, which leaves plenty of room for z-motion. As shown in Fig. 3(a), if the metal layers on the stators and rotors are electrically connected, respectively, the CMOS comb drive functions just like a lateral-axis polysilicon comb drive. On the other hand, if all three metal layers in the rotors are electrically connected while the metal-1 and metal-3 in the stators are separately connected, two sidewall capacitors, C1 and C2, are formed, as shown in Fig. 3(b). If a voltage is applied across C1 or C2, the rotor will move and the device operates as a z-axis actuator.

In order to numerically evaluate the capacitance and expected displacement, a finite element analysis tool, the Maxwell 2D field simulator [11], is employed. The calculated C1 and C2 in Fig. 3(b) and their gradients versus z-displacements are shown in Figure 4. Note that the maximum displacement range is defined by the intersections of the two gradient curves with the zero-gradient line in Figure 4 which occur at -1.4 µm and 2.6 µm, respectively. The electrostatic force F_e is equal to

$$F_e = \frac{1}{2} NL \frac{dC}{dz} V^2 \qquad (1)$$

where N is the number of comb fingers, L the engaged length of comb fingers, and V the applied voltage. The relationship between displacements and required voltages can be obtained by numerically solving the force balance equation, i.e., $F_e = F_{spring} = kz$, where k is the spring constant and z is the z-displacement. The result is plotted in Figure 5 for a series of spring constants. Z-displacement tends to saturate at -1.4 µm and 2.6 µm when the voltage increases.

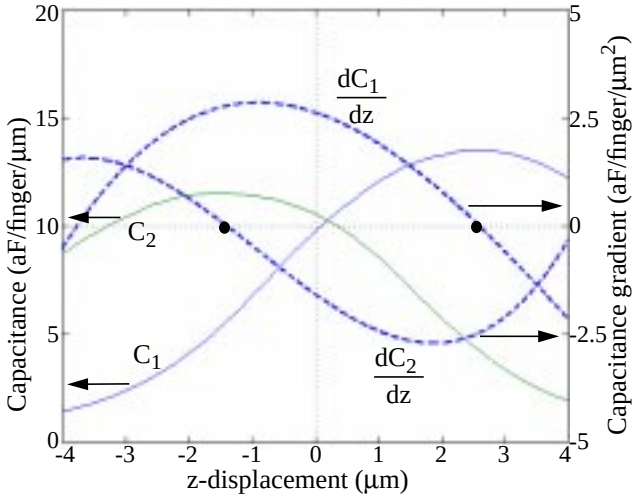

Figure 4: Capacitance and capacitance gradient vs. z-displacement where N=56, L=30 µm.

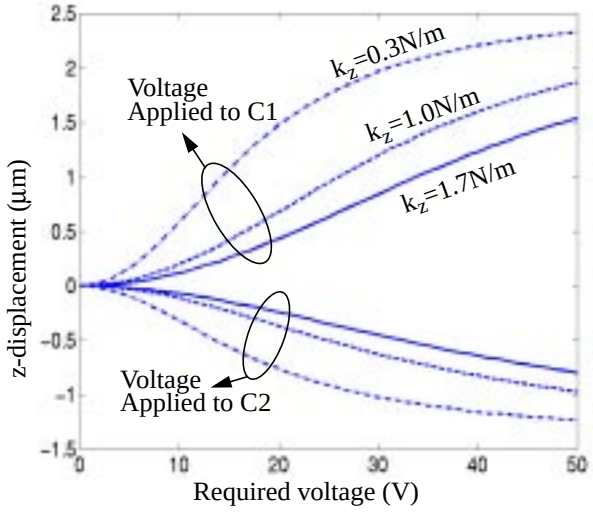

Figure 5: Displacement vs. required voltage.

NODAS SIMULATION

The frequency responses of the device in all three axes are simulated using the NODAS cell library [1]. NODAS (Nodal Design of Actuators and Sensors) is a hierarchical cell library for behavioral modeling and nodal simulation of MEMS. It consists of symbols and models of elements commonly found in suspended MEMS designs, such as anchors, beams and plates. Figure 6 shows the NODAS schematic of the microactuator. The outer curl-matching

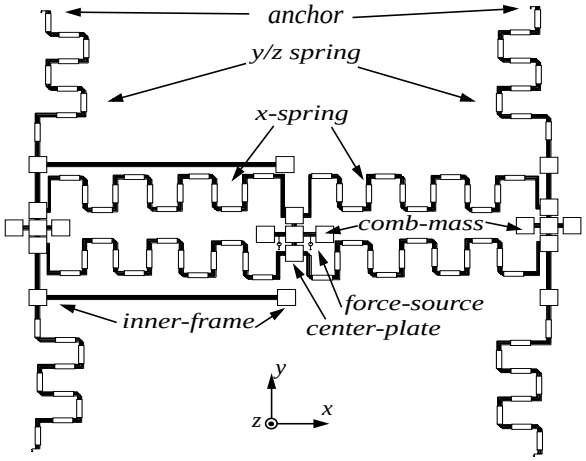

Figure 6: Schematic of the microactuator in NODAS.

frame is rigid enough so that its effect on resonant frequencies of the device is small and is neglected. The inner frame is represented as a series of rigid plates as indicated in Figure 6. The comb drives are simplified to be a series of plates to include the mass of comb fingers, and the device is actuated by an arbitrary external force source of 1 μN instead of electrostatic force. The center plate and x,y/z springs are identified in the schematic. NODAS models for the Hewlett-Packard 0.5 μm CMOS process are used. Mechanical properties of various composite elements are extracted from test structures [10].

The simulation results of resonant frequencies in all 3 axes are listed in Table 1 and compared to the experimental results. The error is within 7%. The simulation and

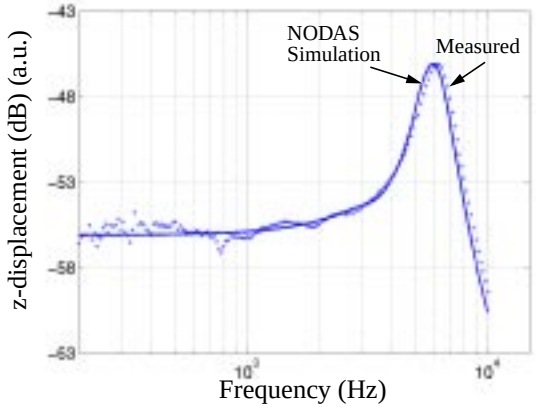

Figure 7: Frequency response in z-axis.

Table 1: Resonant frequencies in x,y,z directions

	Simulation (kHz)	Measured (kHz)	Error
x	22.8	23.8	4.2%
y	4.75	5.08	6.5%
z	5.93	6.17	3.9%

measured results of frequency response in z-axis are plotted in Figure 7, showing excellent agreement across the entire frequency range. The experimental measurements are addressed in the next section.

EXPERIMENTAL RESULTS

The frequency response and z-displacement of the z-axis actuator were measured using a Linnik type Michelson-interferometer system as shown in Figure 8. The microscope objectives image the microstructure and a flat reference mirror simultaneously onto the CCD camera. These two interfering optical fields result in a fringe pattern that allows the evaluation of the topography and real-time displacement measurement. Note that the fringe pattern can be alternatively projected onto a photodiode with a small active area by switching flip mirror 2. The telescope guarantees the uniform illumination of the chosen field of view. To obtain a high intensity fringe pattern, a He:Ne laser (λ = 633 nm) is used to obtain high intensity fringe patterns in the dynamic measurements, while a red LED (λ = 610±10 nm) is employed to avoid speckled images in the static measurements. LEDs also have the advantage of rapid pulsing capability.

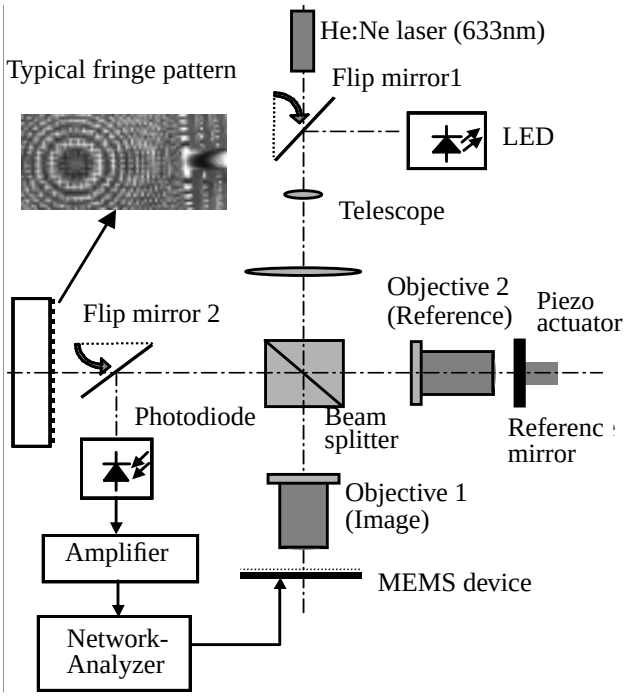

Figure 8: Setup of the Linnik interferometer.

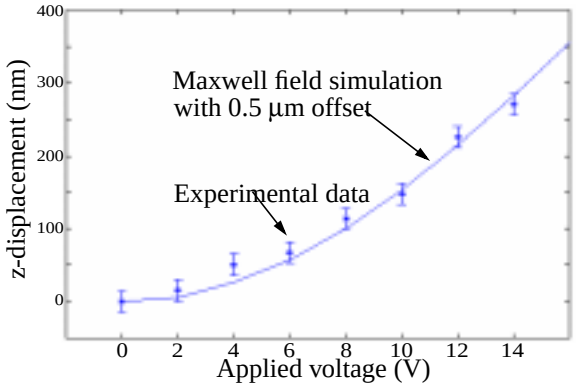

Figure 9: Z-displacements vs. applied voltages.

The relationship among the intensity of the image, microstructure topography and z-displacement is given by

$$I(x, y, z, V) = I_{dc} + I_0 \cos\left[\frac{4\pi}{\lambda} z(V) + \varphi(x, y) + \varphi_0\right] \quad (2)$$

where I is the intensity in the interference pattern, I_{dc} the background intensity, I_0 the amplitude of the intensity modulation in the fringe pattern, λ the wavelength, V the applied voltage, $\varphi(x,y)$ the location-dependent phase change due to the deviation of the microstructure profile from the reference plane, and φ_0 an arbitrary phase. First I_{dc} and I_0 are derived from the interference patterns with the assumption that there is no lateral motion. Then the z-displacement is calculated using Eq. (2). Both the measured and predicted z-displacements versus the applied voltage are plotted in Figure 9. In the field simulation, a 0.1 μm undercut and a 0.5 μm vertical mismatch between rotors and stators were considered. The experimental data fit the theoretical prediction well.

The principle of the z-motion frequency-response measurement is illustrated in Figure 10. The intensity is approximately proportional to the z-displacement when the z-displacement is $< \lambda/10$ and the operating point is near to I_{dc}. The operating point can be adjusted by shifting the reference mirror with the piezo actuator. We use a network analyzer to measure the complex transfer function of the z-actuator (Fig. 7). Since the microstructure is not perfectly flat, the motions in x- and y-directions can also be detected. The measured resonant frequencies in all three directions are listed in Table 1 which shows the NODAS simulation results match the measured values within 7%.

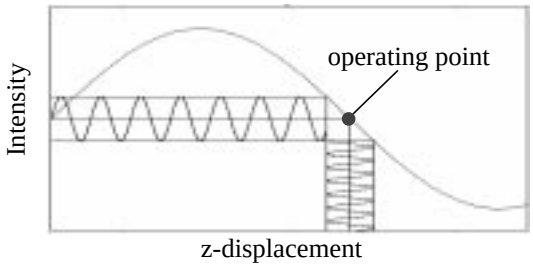

Figure 10: Principe of direct measurement of small z-motion.

CONCLUSIONS

Vertical comb-finger actuation for CMOS MEMS is realized, simulated and tested. For static motion, the Maxwell 2D field simulator is used and the simulation fits the experimental results well. For frequency response, behavioral simulation using the 3-D NODAS library matches the experimental results within 7%. The modeling and simulation is shown to be accurate even for relatively complex multi-conductor microstructures. Moreover, the demonstrated vertical actuation mechanism has potential applications in 3-axis microstage, interferometric systems, lateral-axis vibratory gyroscopes and disk drive heads.

ACKNOWLEDGEMENTS

The authors thank Suresh Santhanam for chip release and SEMs. This research was sponsored by DARPA under the AFRL, Air Force Materiel Command, USAF, under agreement F30602-97-2-0323

REFERENCES

[1] G.K. Fedder, Qi Jing, "A hierarchical circuit-level design methodology for microelectromechanical systems", *IEEE Trans. on Circuits and Systems II*, vol.46, p.1309-15.
[2] W.C. Tang, M.G. Lim, R.T. Howe, "Electrostatically balanced comb drive for controlled levitation", *Tech. Dig. IEEE Solid-State Sensor and Actuator Workshop*, Hilton Head Island, SC, USA; 4-7 June 1990, p.23-7.
[3] G. Zhang, H. Xie, L.E. Derosset, G.K. Fedder, "A lateral capacitive CMOS accelerometer with structural curl compensation", *Proc. MEMS'99*, Orlando, FL, USA; 17-21 Jan. 1999, p.606-611.
[4] Ki Bang Lee, Young-Ho Cho, "Frequency tuning of a laterally driven microresonator using an electrostatic comb array of linearly varied length", *Tech. Dig. Transducers'97*, Chicago, IL, USA; 16-19 June 1997, p.113-16.
[5] W.A. Clark, R.T. Howe, R. Horowitz, "Surface micro-machined Z-axis vibratory rate gyroscope", *Tech. Dig. Solid-State Sensor and Actuator Workshop*, Hilton Head Island, SC, USA; 3-6 June 1996, p.283-7.
[6] M.-H. Kiang, O. Solgaard, K.Y. Lau, R.S. Muller, "Polysilicon optical microscanners for laser scanning displays", *Sensors and Actuators A*, vol.A70, no.1-2, p.195-9.
[7] A.P. Lee, C.F. McConaghy, P.A. Krulevitch, E.W. Campbell, G.E.Sommargren, J.C. Trevino,"Electrostatic comb drive for vertical actuation", *Proc. SPIE*, vol.3224, p.109-19.
[8] G.K. Fedder, S. Santhanam, M.L. Reed, S.C. Eagle, D.F. Guillou, M. Lu, L.R. Carley, "Laminated high-aspect-ratio microstructures in a conventional CMOS process," *Sensors and Actuators A*, vol.A57, no.2, p.103-11.
[9] H. Xie, G.K. Fedder, "A CMOS z-axis capacitive accelerometer with comb-finger sensing", to be presented at MEMS'2000, Miyazaki, Japan, 23-27 Jan. 2000.
[10] M.S.-C. Lu, X. Zhu, G.K. Fedder, "Mechanical property measurement of 0.5 μm CMOS microstructures", *Symp. on Microelectromechanical Structures for Materials Research*, San Francisco, CA, USA; 15-16 Apr.1998, p.27-32.
[11] Maxwell 2D field simulation, Version 1.9.04, Copyright 1984-1997, Ansoft Corporation.